Structure of a polar fluid near a wall. Exact asymptotic behavior of the profile, relation with the electrostriction phenomena and the Kerr effect

J. P. Badiali

Citation: The Journal of Chemical Physics **90**, 4401 (1989); doi: 10.1063/1.456626
View online: http://dx.doi.org/10.1063/1.456626
View Table of Contents: http://scitation.aip.org/content/aip/journal/jcp/90/8?ver=pdfcov
Published by the AIP Publishing

Structure of a polar fluid near a wall. Exact asymptotic behavior of the profile, relation with the electrostriction phenomena and the Kerr effect

J. P. Badiali
Structure et Réactivité aux Interfaces, Université P. et. M. Curie, Batiment F(74), 4 Place Jussieu 75230 Paris Cedex 05, France

(Received 8 August 1988; accepted 15 December 1988)

We study the asymptotic behavior of the position-orientation profile $\rho(1)$ for a dipolar hard sphere fluid in contact with a neutral hard wall. First, by a virial expansion we show that $\rho(1)$ is not totally determined by the classical image potential, i.e., by a dielectric continuum model. The exact expression of $\rho(1)$ far from the wall is derived by using a renormalized cluster expansion. As predicted by the dielectric continuum model, $\rho(1)$ exhibits an orientational structure and a long tail which decreases as the inverse cubic power of the distance to the wall. We first examine the density profile $\rho^0(1)$ which corresponds to the isotropic part of $\rho(1)$. We show that $\rho^0(1)$ contains a part reminiscent of the image potential but also some contributions which depends on the pair correlation function and the triplet direct correlation function in bulk phase. When this last function is neglected, $\rho^0(1)$ can be considered as the result of a force balance in the interface. In the general result, the triplet direct correlation allows us to obtain a very compact expression for $\rho^0(1)$. It is shown that the asymptotic behavior of $\rho^0(1)$ reveals the same microscopic properties as the classical electrostriction phenomena which is observed in bulk phase and in presence of an external electric field. Thus, $\rho^0(1)$ can be considered as the result of a natural electrostriction induced in the interfacial region by the image potential. The term of lowest symmetry in the orientational structure describes the alignment of a molecule relative to the normal to the wall. Far from the wall, the orientational profile is proportional to the dipolar contribution of the Kerr constant. Thus, the asymptotic behavior of the profile and the Kerr effect are determined by the same function characterizing the alignment of dipoles. This alignment is observed via an external field in the case of the usual Kerr effect and it is naturally induced by the image potential in the interfacial region. The triplet direct correlation function gives rise also to some additional orientational structures which are ignored in the dielectric continuum model. The exact results derived in this paper include some bridge diagrams and consequently they are beyond the wall–particle hypernetted chain approximation.

I. INTRODUCTION

The structure of a polar fluid near a hard wall can be described by the position–orientation profile $\rho(1)$ which gives the probability of finding a molecule at a given position in the interface and with a given orientation for its dipole moment. For the dipolar hard sphere fluid near a neutral wall, $\rho(1)$ has been investigated by Monte Carlo simulations,[1] by a renormalized cluster expansion,[2,3] or by integral equation theories.[4] It has been established that $\rho(1)$ exhibits an orientational structure. The origin of this phenomena can be qualitatively understood in terms of classical image potential.[2,3] The interaction of a molecule 1 with the rest of the liquid can be modeled by introducing a dielectric continuum. Since the surface creates a discontinuity in the dielectric permittivity, from classical electrostatics we know that the molecule is submitted to an image potential $U(1)$. If the wall permittivity is unity, then we have

$$U(1) = \frac{\mu^2}{16}\frac{\epsilon - 1}{\epsilon(\epsilon + 1)}(1 + \cos^2\theta_1)/z_1^3, \qquad (1)$$

where ϵ is the dielectric constant of the bulk liquid, μ the magnitude of the dipole moment, z_1 is the distance from the wall, and θ_1 is the polar angle of the dipole measured from the normal to the wall. When the number density ρ of the liquid goes to zero, it has been shown[2,3] that, far from the wall, $\rho(1)$ is given by $1 - \beta U_0(1)$ where β has its usual meaning and $U_0(1)$ is the limit of $U(1)$ to the lowest order in ρ. [Here $\rho(1)$ is normalized in such a way that $\rho(1) = 1$ in bulk phase.] This result also shows a second typical feature of $\rho(1)$, it exhibits a long tail decreasing as $1/z_1^3$.

The aim of this paper is to obtain the exact expression of $\rho(1)$ far from the wall. In order to do that we use a method based on a cluster expansion of $\rho(1)$. In the next section we define the system that we consider and we pursue the low density analysis of $\rho(1)$. The diagrammatic expansion of $\rho(1)$ is then compared to the virial expansion of $1 - \beta U(1)$. We will see that the profile is certainly not totally determined by the image potential. In Sec. III, we generalize the graphs studied at low density. This is done in two steps. First, we replace the Mayer functions by some renormalized bonds. Secondly, we show that the graphs which determine the long tail of $\rho(1)$ at low density represent the first elements of a large class of graphs. The summation of these graphs is done in Sec. IV where the exact expression of $\rho(1)$ is derived. In Sec. V, we discuss the density profile $\rho^0(z_1)$ which is obtained from $\rho(1)$ by an averaging over the molecular orientations. Particularly, we will examine the possibility to obtain $\rho^0(z_1)$ from macroscopic considerations and we shall see that the asymptotic behavior of the profile is related to the electrostriction phenomena. Finally, in the last sec-

 0021-9606/89/084401-12$02.10

tion, we will focus on the orientational structure which persists far from the wall. In this case we will consider essentially the alignment of dipole relative to the wall and we emphasize its relation with the usual Kerr effect which is observed in bulk phase and in presence of an external field.

Some mathematical aspects of this work will be given in Appendices.

II. DEFINITION OF THE SYSTEM AND THE LOW DENSITY ANALYSIS

We consider a planar interface (see Fig. 1). $\hat{z}$ is the unit vector in the direction normal to the wall. The wall–molecule interaction is given by

$$U_w(i) = U_w(z_i) = \begin{cases} \infty & \text{if } z_i < 0 \\ 0 & \text{if } z_i > 0 \end{cases} \quad (2)$$

Thus, the center of molecules is confined in the half-space defined by $z>0$. For the sake of simplicity we will stay with the dipolar hard sphere model. Then, the pair potential between two particles i and j is given by

$$U(i,j) = V^s(i,j) + V^l(i,j), \quad (3)$$

where $V^s(i,j)$ is the hard sphere potential

$$V^s(i,j) = \begin{cases} \infty & \text{if } r_{ij} < \sigma \\ 0 & \text{if } r_{ij} > \sigma \end{cases} \quad (4)$$

σ is the hard sphere diameter. In Eq. (3), $V^l(i,j)$ is the dipole–dipole interaction

$$V^l(i,j) = \mu^2[\hat{\mu}_i\cdot\hat{\mu}_j - 3(\hat{\mu}_i\cdot\hat{r}_{ij})(\hat{\mu}_j\cdot\hat{r}_{ij})]/r_{ij}^3$$
$$= \mu^2(\hat{\mu}_i\cdot\nabla_i)(\hat{\mu}_j\cdot\nabla_j)1/r_{ij}, \quad (5)$$

where $\hat{\mu}_i$ and $\hat{\mu}_j$ are the unit vectors in the direction of the dipole moments, $\hat{r}_{ij}$ is the unit vectors in the direction $\mathbf{r}_{ij}$ joining the center of the particles, and ∇_i is the gradient operator acting on the spatial coordinates of i.

In order to calculate the profile $\rho(1)$, we start from the usual method in which the planar hard wall is considered as the limit of a giant spherical particle.[5,6] To the potentials defined in Eqs. (2) and (3), we associate the corresponding Mayer functions. Between the wall–particle here referred by 0 and a molecule i we have

$$f_w(i) = \exp -\beta U_w(0,i) - 1, \quad (6)$$

where $U_w(0,i)$ has $U_w(i)$ as limit when the radius of the giant particle grows infinitely. The Mayer function relative to polar molecules is given by

$$f(i,j) = \exp -\beta U(i,j) - 1, \quad (7)$$

As observed in Refs. 2–4, classical electrostatics plays a central role in our problem. Particularly, we have seen that $U(1)$ determines the exact behavior of $\rho(1)$ at very low density. Since $U(1)$ is obtained for a point dipole, we introduce

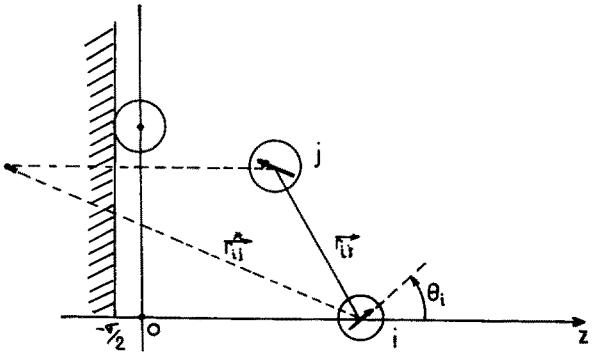

FIG. 1. Description of the interface and definition of geometrical variables. The "physical" wall is located at $z = -\sigma/2$. The distance r_{ij}^* introduced in Eq. (29) is obtained by mirroring z_j relatively to the plane $z=0$.

in $f(i,j)$ a part $f^l(i,j)$ which is as close as possible to the point dipole model. This can be done by introducing around each dipole an excluded volume having an infinitesimally small radius λ.[7] Now, we write $f(i,j)$ as

$$f(i,j) = f^s(i,j) + f^l(i,j), \quad (8)$$

where $f^l(i,j)$ is defined as in Ref. 7 by

$$f^l(i,j) = -\beta\theta(r_{ij}-\lambda)\mu^2(\hat{\mu}_i\cdot\nabla_i)(\hat{\mu}_j\cdot\nabla_j)1/r_{ij}, \quad \lambda\to 0. \quad (9)$$

$\theta(x)$ is the Heaviside step function [$\theta(x)=0$ if $x<0$ and $\theta(x)=1$ if $x>0$]. At the end of our calculations we will take the limit $\lambda\to 0$. The function $f^l(i,j)$ is independent of the hard sphere diameter. It represents a purely electrostatics quantity. We may consider $f^l(i,j)$ as the sum of two distributions noted

$$\phi_d(i,j) = -\beta\mu^2(\hat{\mu}_i\cdot\nabla_i)(\hat{\mu}_j\cdot\nabla_j)1/r_{ij}, \quad (10)$$

$$\phi_e(i,j) = (4\pi\beta\mu^2/3)\hat{\mu}_i\cdot\hat{\mu}_j\delta(r_{ij})/r_{ij}^2, \quad (11)$$

where $\delta(r_{ij})$ is the one-dimensional dirac function and $\phi_d(i,j)$ is defined in Appendix A.

In Eq. (8), $f^s(i,j)$ can be split in a pure hard sphere part $f^{s0}(i,j)$ and a dipolar contribution $f^{sd}(i,j)$. They are defined by

$$f^{s0}(i,j) = \theta(r_{ij}-\sigma) - 1,$$
$$f^{sd}(i,j) = -\beta[\theta(r_{ij}-\sigma) - \theta(r_{ij}-\lambda)]$$
$$\times\mu^2(\hat{\mu}_i\cdot\nabla_i)(\hat{\mu}_j\cdot\nabla_j)1/r_{ij} + \theta(r_{ij}-\sigma)$$
$$\times\sum_{n\geq 2}[-\beta\mu^2(\hat{\mu}_i\cdot\nabla_i)(\hat{\mu}_j\cdot\nabla_j)1/r_{ij}]^n/n! \quad (12)$$

By using the classical cluster expansion method,[8] $\rho(1)$ can be calculated in terms of Mayer functions. Here, $\rho(1)$ is formally the radial distribution function between the wall particle and a polar molecule. We have

$\rho(1) = 1 +$ sum of all distinct graphs in which we have two root points noted 0 and 1 of weight 1. From 0 starts, at least, one f_w bond. The field points, weighted by ρ, can be connected by a f^s or a f^l bond in such a way that the graph is free of articulation points. (13)

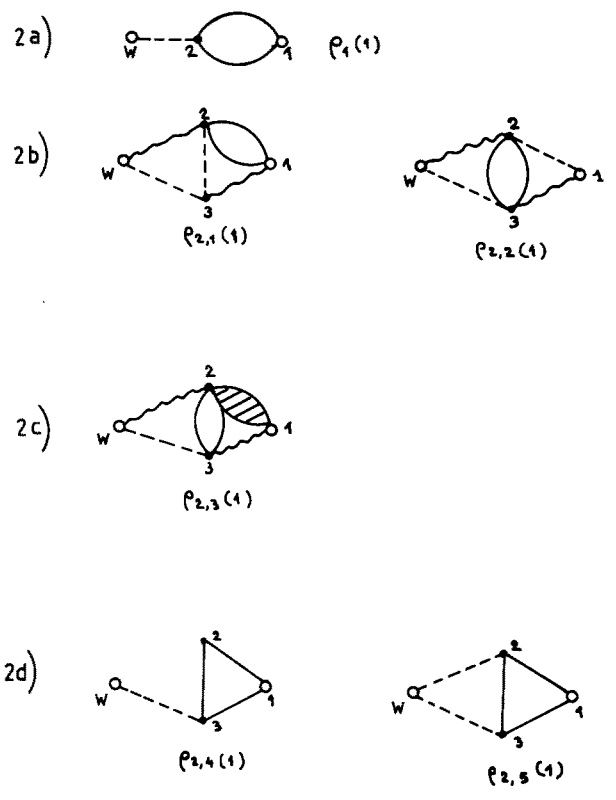

FIG. 2. The low density expansion of $\rho(1)$: graphs giving a contribution to the asymptotic behavior of $\rho(1)$. The graph in (a) corresponds to the order ρ while those in (b), (c), and (d) contribute to the order ρ^2. In this figure, — represents a f^l bond, --- is a hard sphere bond (f_w or f^{s0}), and the wavy line represent $(1+f_w)$ or $(1+f^{s0})$. In (c) the hachured connection corresponds to f^{sd}.

In this section we study the density expansion of $\rho(1)$ and we will focus on its asymptotic behavior far from the wall. To each order in ρ, the profile can be also expanded in power series of μ. Hereafter, we consider this double expansion. The first term noted $\rho_1(1)$, corresponds to the order ρ. It has been already discussed in Refs. 2 and 3 and its diagrammatic representation is given in Fig. 2(a). In Appendix B we show why this kind of graph may contribute to the long tail of the profile. From Ref. 3, we have

$$\rho_1(1) = -\beta\mu^2 3y(1+\cos^2\theta_1)/(32z_1^3), \tag{14}$$

where y is the usual variable defined by $y = 4\pi\rho\beta\mu^2/9$.

The graphs corresponding to the order ρ^2 have two field points, some of them are shown in Figs. 2(b), 2(c), and 2(d) and their contribution to $\rho(1)$ is $\rho_2(1)$. Among the graphs of $O(\rho^2)$ those with only one f^l bond vanish. In this case, at least one end of f^l is a field point and then, the integration over the dipolar orientation cancels the graph. Graphs with two f^l bonds do not vanish provided the f^l bonds are connected in parallel as shown in Fig. 2(b). In addition to these f^l bonds the graphs can be decorated by some f_w and f^s bonds. When f^s is reduced to its hard sphere part f^{s0}, we obtain the graphs of lowest order in $\beta\mu^2$, they are drawn in Fig. 2(b). In the first one noted $\rho_{2,1}(1)$ the molecule 2 is on the liquid side while 3 is inside the wall. Due to the short-range bond connecting 2 and 3, 3 must be in close proximity to 2. Accordingly, these two molecules explore a limited region of space located near the wall and, from the discussion given in Appendix B, we conclude that $\rho_{2,1}(1)$ does not contribute to the long tail of $\rho(1)$. By using similar arguments, we can see that the second graph noted $\rho_{2,2}(1)$ [see Fig. 2(b)] must be retained.

The calculation of $\rho_{2,2}(1)$ far from the wall is straightforward. Since molecules 1 and 2 are very close ($r_{12}<\sigma$) and 1 very far from the wall, i.e., $z_1 \gg \sigma$, 2 is necessarily far from the wall too. Then, after the integration over 3, 2 is related to the wall by $\rho_1(2)$. The bond between 1 and 2 selects the isotropic part $\rho_1^0(z_2)$ of $\rho_1(2)$, obtained from Eq. (14) by an averaging over the dipolar orientations. We get $\rho_1^0(z_2) = -\beta\mu^2 y/(8z_2^3)$. The calculation of $\rho_{2,2}(1)$ results now from a convolution over the spatial coordinates of $\rho_1^0(z_2)$ and $f^{s0}(2,1)$. It can be performed easily by expanding $\rho_1^0(z_2)$ around $\rho_1^0(z_1)$. The first term is simply given by the product $\rho_1^0(z_1)(-4\pi\rho\sigma^3/3)$. The other terms in the expansion decrease more rapidly than $1/z^3$ and the final result is simply $\rho_{2,2}(1) = 3y^2(\sigma/z_1)^3/8$. (A precise mathematical justification of this result is given in Appendix B.) We observe that this contribution to $\rho(1)$ does not depend on the orientations of 1. The arguments developed here are similar to those already used in studies concerning the structure of homogeneous polar fluids (see, for instance, Ref. 9).

In the graph associated to $\rho_{2,2}(1)$ we may replace $f^{s0}(2,1)$ by $f^{sd}(1,2)$ defined in Eq. (12). Thus, we introduce a contribution of higher order in $\beta\mu^2$. As a consequence of the well known "parity selection rule" which establishes that the number of bonds emerging from a field point must be necessarily even,[10] we conclude that the graph given in Fig. 2(c) is, at least, proportional to $\rho^2(\beta\mu^2)^4$. As opposed to $\rho_{2,2}(1)$, this new graph will be depending on the orientation of 1. From the arguments presented in Appendix B, this graph can be calculated in the same way that $\rho_{2,2}(1)$ is. The result [see Eq. (B10)] is essentially determined by the product of $\rho_1(1)$ by the integral of $f^{sd}(1,2)$ on the overall space.

However, some graphs with only three f^l bonds exist, they are drawn in Fig. 2(d) and noted $\rho_{2,4}(1)$ and $\rho_{2,5}(1)$. Such graphs can be calculated exactly by using transverse Fourier transforms [as an illustration, the calculation of $\rho_{2,5}(1)$ is presented in Appendix C] and their contributions to $\rho(1)$ is

$$\rho_{2,4}(1)+\rho_{2,5}(1) = 9y^2\beta\mu^2(1+\cos^2\theta_1)/(64z_1^3). \tag{15}$$

Finally, the net result for $\rho_2(1)$ can be written

$$\rho_2(1) = 3y^2(\sigma/z_1)^3/8 + 9y^2\beta\mu^2 \times(1+\cos^2\theta_1)/(64z_1^3)+\cdots. \tag{16}$$

Where the dots represent some terms of the form $y^2(\beta\mu^2)^n$ with $n>2$. By adding Eqs. (14) and (16) we find for the asymptotic behavior of the profile

$$\rho(1) = 1 - 3y\beta\mu^2(1-3y/2)(1+\cos^2\theta_1)/(32z_1^3) + 3y^2(\sigma/z_1)^3/8+\cdots. \tag{17}$$

Now, we compare Eq. (17) to the low density expansion of $-\beta U(1)$. From the recent works concerning the so called dielectric virial expansion,[11–13] we know that the dielectric constant ϵ can be written as

$$\epsilon = 1 + 3y + 3y^2(1+b) + O(\rho^3), \tag{18}$$

where b is related to the second dielectric virial coefficients for which an exact expression has been found.[11] The coefficient b only depends on the value of the reduced dipole moment $\beta\mu^2/\sigma^3$ and the first term in the expansion of b corresponds to $(\beta\mu^2/\sigma^3)^4$. When expansion (18) is introduced into Eq. (1), we get

$$1-\beta U(1)=1-3y\beta\mu^2(1-7y/2)\times(1+\cos^2\theta_1)/(32z_1^3)+\cdots. \quad (19)$$

This result is obtained by selecting, to each order in ρ, the terms corresponding to the lowest order in $\beta\mu^2$. The comparison of Eqs. (17) and (19) reveals two important discrepancies in the expansions: (i) the last term in Eq. (17) represents a combination of y and μ^2 which does not exist in Eq. (19) and (ii) the terms of order $y^2(\beta\mu^2)$ which are present in Eqs. (17) and (19) do not have the same coefficient.

Thus, from the low density analysis we may conclude that the long tail of $\rho(1)$ is certainly related to the existence of an image potential but this effect is not the only one which dictates the asymptotic behavior of $\rho(1)$.

III. SELECTION OF GRAPHS

At a density corresponding to the liquid state the calculation of $\rho(1)$, as that of any other quantity, requires the evaluation of an infinite sum of graphs. In this section our main task consists of finding the graphs which give rise to the peculiar behavior of the profile. In Appendix B we have found the mathematical conditions which lead to the existence of a long tail in $\rho(1)$. Obviously, these conditions are fulfilled by the graphs analyzed in the previous section and here we will try to generalize these graphs. In order to do that we will proceed step by step. First, we carry out a topological reduction which allows us to replace a f^l bond by an infinite sum of graphs having the same spatial dependence. In a second step, we will see that some diagrammatic structures studied at low density $[\rho_1(1), \rho_{2,5}(1)]$ represent the first elements of a general class of graphs. The other graphs considered above $[(\rho_{2,2}(1), \rho_{2,3}(1)]$ result from a convolution including $\rho(1)$ and a short-ranged correlation function in the bulk phase. Besides the renormalization of the long-range bonds, we realize a second topological reduction which leads to replacing an usual field point by an hypervertex. Thus, we introduce in the calculation of $\rho(1)$ an infinite sum of graphs related to the short-ranged structure in the bulk liquid.

A. Renormalization of the long-range bonds

In Sec. II it has been shown that the long tail of $\rho(1)$ results from particular combinations of bonds which decrease as the inverse cubic power of the distance between the particles. This spatial dependence which characterizes the dipolar potential also appears when we consider some chains of dipole–dipole bonds.[7,9,14–17] We know that such chains determine the long-range behavior of the total pair correlation function $h(1,2)$. Thus, it must be possible to include directly in the calculation of $\rho(1)$ a part of $h(1,2)$. Before doing that we briefly summarize some properties of $h(1,2)$ in bulk phase. Here, we use essentially the formalism of Høye and Stell.[17]

The total correlation function $h(1,2)$ can be separated in a short-range part $h^s(1,2)$ and a long-range part $h^l(1,2)$, the γ-ordering procedure gives us a precise criteria for performing such a separation. The long-range part $h_l(1,2)$ results from the infinite sum of chains of f^l bonds. In these chains, to each field point i is associated an hypervertex which takes into account the polarization induced by the molecule i in its neighborhood. The properties of the hypervertex are essentially determined by the short range function $h^s(i,j)$. In homogeneous liquids the hypervertex leads to a scaling in the magnitude of the dipole moment.

The function $h^l(1,2)$ can be written as

$$h^l(1,2)=\frac{(1+B/3)^2}{(1+2z)(1-z)}\phi_d(1,2)+\frac{(1+B/3)}{(1-z)}\phi_e(1,2), \quad (20)$$

where ϕ_d and ϕ_e have been defined in Eqs. (10) and (11), respectively. In Eq. (20), the parameter z is related to the dielectric constant ϵ by a Clausius–Mosotti type equation

$$z=(\epsilon-1)/(\epsilon+2) \quad (21)$$

and between z, y, and B we have the relation

$$z=y(1+B/3) \quad (22)$$

In order to combine properly long-range bonds, hypervertices, and f_w bonds we define two renormalized bonds by

$$D(1,2)=\frac{1}{(1+2z)(1-z)}\phi_d(1,2), \quad (23)$$

$$E(1,2)=\frac{1}{(1-z)}\phi_e(1,2), \quad (24)$$

and their sum

$$C(1,2)=D(1,2)+E(1,2). \quad (25)$$

$C(1,2)$ represents, in bulk phase, the sum of all chains formed of f^l bonds, each field point is weighted by $\rho(1+B/3)$ while the ending points have a weight unity. In other words, in all chains which give rise to C, the bonds emerging from the root points are necessarily of f^l type. The comparison of Eqs. (20) and (25) shows that $h^l(1,2)=(1+B/3)^2C(1,2)$.

Clearly, since the renormalized bond $C(1,2)$ has the same long-range behavior as $f^l(1,2)$, when $C(1,2)$ is substituted to $f^l(1,2)$ it will give the same kind of contribution to $\rho(1)$. For example, in the graph given in Fig. 2(a) we replace each $f^l(1,2)$ by $C(1,2)$. We may immediately verify that this new graph pertains to the cluster expansion of $\rho(1)$ given in Eq. (11). Moreover, its contribution to $\rho(1)$ is simply proportional to $\rho_1(1)$ given in Eq. (12). Now, we may still generalize this new graph in two ways.

B. Ring of f^l bonds and short-ranged correlations

By analogy with the custer theory of ionic solutions,[8,18] we can say that the graph given in Fig. 2(a) has, relative to its long range bonds, a ring structure. Clearly, it represents the most simple ring since it has the minimum number of bonds. The graph associated to $\rho_{2,5}(1)$ represents another element having a ring structure. A general class of ring graphs can be generated by introducing a renormalized bond $C(i,j)$ instead of $f^l(i,j)$ and by increasing the number of $C(i,j)$ bonds in the ring. However, in order to create a new graph, i.e., a graph distinct from the

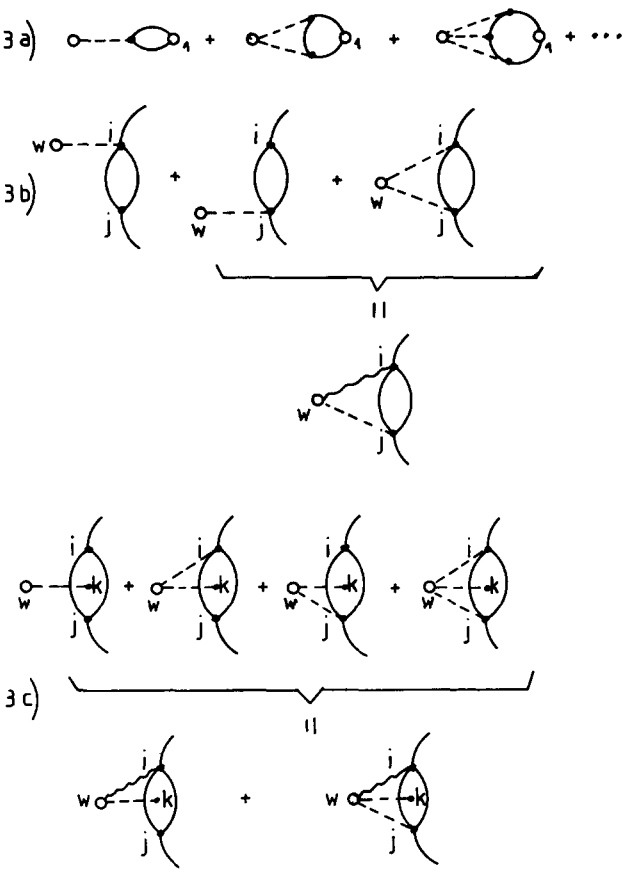

FIG. 3. Generalization of graphs studied in Sec. II. — represents a renormalized bond C defined in Eqs. (23)–(25), --- represents a f_w bond, and the wavy line $(1+f_w)$. In (a) we increase the number of renormalized C bond in the ring, the field points are weighted by ρ. In (b) we insert between i and j the short-range bond corresponding to the first term in Eq. (26), the last two graphs are added. (c) represents the graphs associated to the short-ranged connection corresponding to the second term on the right-hand side of Eq. (26).

previous ones, two adjacent C bonds must be necessarily connected to the wall as indicated in Fig. 3(a). Thus, the introduction of an extra C bond in the ring is equivalent to increasing the number of connections $[f_w(i)]$ with the wall and the new graphs are distinguishable by the number of such connections. For instance, we see that the graphs given in Fig. 3(a) are topologically different.

From the definition of C, we may generalize these rings by inserting a short-range bond between two long-range ones. In order to go further in the discussion we must distinguish two cases depending on whether the short-range bond is related to the wall or to the root point 1. The third possibility, in which a short-range bond should be related both to the wall and to 1 can be dropped since, as 1 is very far from the wall, clearly such a kind of graph can not contribute to the long-range tail of $\rho(1)$. We first analyze the case where the short-range bond is related to the wall.

We consider two C bonds arriving at the field points i and j as indicated in Fig. 3(b). The particular case in which $i=j$ corresponds to Fig. 3(a), it can be represented by a bond $\delta(i,j)/\rho(i)$ where the dirac function $\delta(i,j)$ acts both on the spatial and angular coordinates of i and j. Besides this trivial short-range bond, we may insert between i and j a more general connection $F(i,j)$. This function has to verify simultaneously the two conditions: (i) $F(i,j)$ must be short ranged in order to be different from a $C(i,j)$, and (ii) $F(i,j)$ must be related to the wall at least once by a f_w bond in order to be different from the hypervertex existing in a C bond. Clearly a graph different from those given in Fig. 3(a) is then created. Now, we construct $F(i,j)$ from the total pair correlation function $h^s(w,i,j)$ in the presence of the wall. At least formally, $h^s(w,i,j)$ can be calculated by a functional expansion around its bulk expression $h^s(i,j)$. We have

$$h^s(w,i,j) = h^s(i,j) + \int \frac{\delta h^s(i,j)}{\delta\rho(k)} f_w(k)\,dk + \cdots; \quad (26)$$

When the first term is retained, we obtain $F(i,j)$ by adding one or more f_w bonds. This can be done in three different ways as shown in Fig. 3(b). When focusing on the long-range behavior of $\rho(1)$, it is useful to add these graphs. However in such an operation we must take into account the symmetry number n of the graph. If the addition of f_w bonds does not change n, two graphs can be simply added as shown in Fig. 3(b). Then, in the resulting graph, we see that i is now outside the wall while j is inside. Accordingly due to the short-range bond, $h^s(i,j)$, i and j remain near the wall and from the arguments developed in Appendix B, this graph does not contribute to the long tail of $\rho(1)$. Consequently, the net contribution to $\rho(1)$ is then given by the remaining graph in Fig. 3(b). If the introduction of f_w bonds changes the symmetry number n, the addition of graphs is still possible and some graphs can be eliminated as above. By pictorial arguments, it is easy to verify that the net result corresponds to a graph with only one connection to the wall and the graph has the higher symmetry number. Thus, when $h^s(i,j)$ is inserted between i and j we recover the situation encountered in homogeneous systems except that i or j is inside the wall. By the usual arguments[9,17,19] we may combine this $F(i,j)$ to $\delta(i,j)/\rho(j)$ in a hypervertex which is precisely the one corresponding to the bulk phase. Accordingly, the field points are now weighted by $\rho(1+B/3)$.

In the second term of the expansion (26), the functional derivative is obtained from $h^s(i,j)$ by taking all ways of turning one field point in a root point here labeled $k(k\neq i$ or $j)$. The most general expression of $F(i,j)$ will be obtained by adding 0, 1, or 2 f_w bonds connecting i and j to w as shown in Fig. 3(c). These graphs can be added as discussed previously. Now, k is necessarily inside the wall while i or j are outside. Thus, this kind of graph does not contribute to the long tail of $\rho(1)$. Once again, by pictorial arguments, we can check that this result remains whatever the symmetry number of the graph. Hence, for determining $\rho(1)$, we have to calculate the infinite sum of ring graphs formed of C bonds, these bonds are connected to the wall by $\rho(1+B/3)f_w(i)$.

Now, we examine the case where a short-range bond relates i,j and the root point 1. The most simple situation corresponds to the Fig. 3(a) where $i\equiv j\equiv 1$ [see also Fig. 4(a)]. By analogy with the discussion presented above we may represent this configuration by a product of delta bonds $\delta(i,1)\delta(j,1)/\rho(i)\rho(j)$. The introduction of a more general short-range bond $F(1,i,j)$ can be discussed in terms of nodal point which is of common use in the cluster theory.[8] If 1 is a nodal point, then between 1 and i on one hand and 1 and j on the other hand we can introduce independently all sums of graphs provided the sum is short ranged. The infinite sum

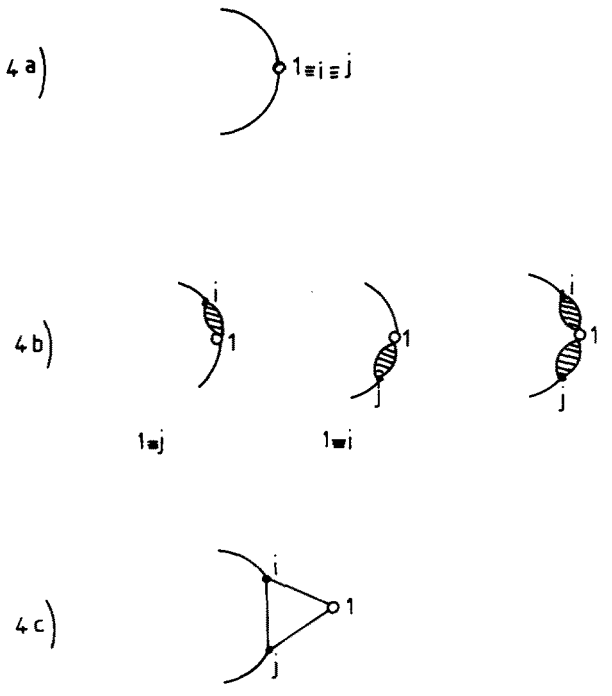

FIG. 4. Connection with the root point 1. — represents a C bond. In (a), all points i, j, and 1 are identical. In (b), 1 is a nodal point and the hachured bonds corresponds to h^s. In (c), the triangle represents the direct triplet correlation function between 1, i, and j.

corresponds to the short range part h^s of the total pair correlation function in bulk phase. The combination of h^s and delta bonds give the graphs shown in Figs. 4(a) and 4(b). By the procedure leading to hypervertices[9,17,19] we may replace these graphs by the one corresponding to Fig. 4(a) but multiplied by $(1+B/3)^2$. Now, we consider the opposite case where i and j are connected via a short-range function which is free from nodal point. By definition this function corresponds to the short-range part of the direct correlation function $c(i,j)$ between i and j. In order to obtain $F(1,i,j)$, we must create an extra root point in $c(i,j)$, this is equivalent to taking the functional derivative of $c(i,j)$ relative to the function $\rho(k)$ $(k \neq i,j)$ and to label this new point 1. This derivative is nothing less than the triplet direct correlation function $c(1,i,j)$ between i,j and 1[20] [see Fig. 4(c)]. This function induces some correlations between a particle inside the wall and three particles on the liquid side via a bridge diagram. More generally, the Fig. 4 illustrates various kinds of coupling between the particle 1 and the "wall." In Fig. 4(a) we may consider that we have a direct coupling while in Figs. 4(b) and 4(c) the existence of the wall, i.e., the presence of a large excluded volume, is transmitted to 1 via its short range environment. An analogous situation is encountered in the microscopic theory of the electrostriction.[21]

In summary, we have seen that the graph given in Fig. 2(a) can be generalized in different ways. First, each $f^l(i,j)$ bond can be replaced by a renormalized bond $C(i,j)$ which is proportional to the long range part $h^l(i,j)$ of the total correlation function $h(i,j)$ in bulk phase. Secondly, by increasing the number of C bonds we generate a ring structure in which each field point i is weighted by $\rho(1+B/3)$. In doing that we have introduced the short-range part $h^s(i,j)$ of $h(i,j)$. Finally, the root point 1 can be inserted in the ring in two ways: (i) directly [Fig. 4(b)], with a weight $(1+B/3)^2$ or (ii) via a triplet direct correlation function $c(1,i,j)$ as shown in Fig. 4(c). In all these graphs we have assumed that the connection with the wall is only determined by f_w. A more general situation will be considered below in Sec. IV A.

Now, we consider the generalization of the graphs given in Figs. 2(b) and 2(c) and corresponding to $\rho_{2,2}(1)$ and $\rho_{2,3}(1)$.

C. Convolution including a ring graph and the Ornstein–Zernike equation

In Sec. II we have seen that $\rho_{2,2}(1)$ results from a convolution between $\rho_1(2)$ which is a ring graph and a short range bond $f^{s0}(1,2)$. The calculation of $\rho_{2,3}(1)$ given in Fig. 2(c) can be performed by the same procedure. More generally, we may relate 2 to 1 by the total pair correlation function in the bulk phase $h(1,2)$ since no restriction exists on this connection. However, as a consequence of the parity selection rule, only a part of $h(1,2)$ will be retained. In $\rho_{2,2}(1)$ and $\rho_{2,3}(1)$ only the short-range part in the expansion of $h(1,2)$ is kept. Thus, in addition to the ring graph we also consider the convolution of a ring graph ending at the field point 2 with $h(2,1)$. This corresponds to the situation investigated in Appendix B [see Eq. (B8)].

By construction, 2 is a nodal point. The graphs considered here can be analyzed with respect to the existence of such points. We know that this analysis relates the cluster expansion to the classical Ornstein–Zernike equation.[8] In our case, where the formalism of the giant particle is used, we must replace each graph considered above in the expansion of $h(1,2)$ or $c_w(0,1)$, which is the direct correlation function between the wall particle (0) and a polar molecule (1). For instance in Fig. 2(a), $c_w(0,1)$ is approximated by $f_w(1)$ and $h(1,2)$ by $[f^l(1,2)]^2/2$. When a ring has more than one field point, it represents a graph in which 0 and 1 are, at least, doubly connected and consequently these rings pertain to the expansion of $c_w(0,1)$. The graphs which arrive at the root point via the triplet direct correlation function [Fig. 4(c)] represent the contribution of some bridge diagrams to $c_w(0,1)$.

In the next section, we shall see that all graphs selected contribute to the long-range tail of $\rho(1)$ and their infinite sum will be calculated.

IV. EXACT ASYMPTOTIC BEHAVIOR OF THE PROFILE

At the end of Sec. III B, we have summarized the properties of a ring. They suggest a step by step procedure in the calculation of their infinite sum. First, we consider the infinite sum of chain graphs $S(k,l)$ in which all points are inside the wall as shown in Fig. 5(a). In the second step, each ending point (k or l) will be connected via a C bond to a point (i or j) located in the liquid but far from the wall (see Fig. 5). Finally, i and j will be identified to the root point 1 or related to 1 via the triplet direct correlation function. To the ring contribution we have to add the convolution introduced in Sec. III C.

A. Chain calculations

The calculation of the sum $S(k,l)$ defined above can be performed exactly by a method already presented in Ref. 7. The determination of $S(k,l)$ requires the evaluation of some integrals such as

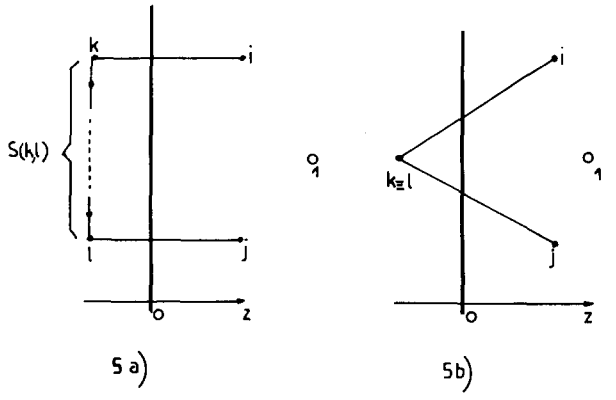

FIG. 5. Chain calculation performed in Sec. IV A. — represents a C bond. In (a), $S(k,l)$ is an infinite sum of chain graphs in which all points are inside the wall ($z<0$) which is represented by a vertical line, i and j are on the liquid side far from the wall, i and j have to be connected to the root point 1 in different way. In (b) we have the same elements but $S(k,l)$ is replaced by $\delta(k,l)/\rho(l)$.

$$\int C(l,m)\rho(1+B/3)f_w(m)C(m,n)dm \tag{27}$$

The coefficient $\rho(1+B/3)$ results from the introduction of the hypervertex. From Eqs. (23)–(25), each C bond is a linear combination of ϕ_d and ϕ_e defined in Eqs. (10) and (11), respectively, and Eq. (27) leads to calculate the convolution of these distributions. By using a transverse Fourier transform and a calculation analogous to the one presented in Appendix C, the product of ϕ_d bonds can be readily performed, we get

$$\begin{aligned}\phi_d^*\phi_d &= -\rho(1+B/3)\int_{z_m<0}\phi_d(l,m)\phi_d(m,n)dm \\ &= 3z\phi_d-(3z/2)\phi_i.\end{aligned} \tag{28}$$

Where ϕ_i is a distribution similar to ϕ_d but corresponding to the image potential. We have

$$\phi_i = -\beta\mu^2(\hat{\mu}_i\cdot\nabla_i)(\hat{\mu}_j\cdot\nabla_j)1/r_{ij}^*, \tag{29}$$

where r_{ij}^* is deduced from r_{ij} by mirroring z_i (or z_j) relative to the plane $z=0$ (see Fig. 1). In Eq. (27), the parts associated to ϕ_e are immediately calculated and we have

$$\phi_e^*\phi_d = -z\phi_d \text{ and } \phi_e^*\phi_e = -\phi_e. \tag{30}$$

In addition to the products considered in Eqs. (28) and (30), we also have

$$\phi_i^*\phi_i=(3z/2)\phi_i;\quad \phi_e^*\phi_i=-z\phi_i;\text{ and }\phi_d^*\phi_i=(3z/2)\phi_i. \tag{31}$$

The relations (28), (30), and (31) show that ϕ_d,ϕ_i, and ϕ_e form a closed set and the sum $S(k,l)$ can be readily obtained by an iterative procedure. The sum S_n of all chains in which we have, at most, n field points can be written in the form

$$S_n = S_n^d\phi_d + S_n^i\phi_i + S_n^e\phi_e \tag{32}$$

and the sum S_{n+1} corresponds to

$$S_{n+1} = S_{n+1}^d\phi_d + S_{n+1}^i\phi_i + S_{n+1}^e\phi_e \tag{33}$$

or

$$\begin{aligned}S_{n+1} &= \frac{\phi_d}{(1+2z)(1-z)}+\frac{\phi_e}{(1-z)} \\ &\quad + S_n^*\left[\frac{\phi_d}{(1+2z)(1-z)}+\frac{\phi_e}{(1-z)}\right].\end{aligned} \tag{34}$$

The last term in the right-hand side of Eq. (34) can be calculated by using Eq. (32) and the product rules (28), (30), and (31). In the limit $n\to\infty$, we have $S_n\to S_{n+1}$, $S_n^d\to S_{n+1}^d$,...and we may solve Eq. (34). After elementary algebra we obtain

$$\begin{aligned}S(k,l) &= \frac{4\pi\beta\mu^2}{3}\hat{\mu}_k\cdot\hat{\mu}_l\frac{\delta(r_{kl})}{r_{kl}^2}-\beta\mu^2(\hat{\mu}_k\cdot\nabla_k)(\hat{\mu}_l\cdot\nabla_l) \\ &\quad\times\left[\frac{1}{r_{kl}}-\frac{3z}{(z+2)}\frac{1}{r_{kl}^*}\right].\end{aligned} \tag{35}$$

In this calculation, the connection with the wall is given by $f_w(n)$ defined in Eq. (6). In this case, the field point n explores the overall half-space ($z<0$) which is uniformly weighted by -1. A more general connection with the wall can be considered. Then, in addition to previous calculations, we must add some graphs in which n can penetrate in the region $z>0$. However, in these graphs n remains in the interfacial region which is of finite thickness compared to the overall half space. From the γ-ordering arguments developed in Ref. 7, we conclude that these graphs do not contribute to the long-range behavior of $S(k,l)$. Consequently, in our calculations concerning the long tail of $\rho(1)$ the relevant connection with the wall is given by f_w.

B. Connections to the root point 1

Now, we relate $S(k,l)$ to the points i and j in the liquid side [Fig. 5(a)]. In the convolution $S(k,l)*C(l,i)$, the part of $C(l,i)$ which is related to the exclusion, $\phi_e(l,i)$, does not contribute since l and i are in two distinct regions of space. After a straightforward calculation using the transverse Fourier transform, we have

$$S(k,l)*C(l,i) = \frac{z(1-4z)}{(1+2z)(1-z)(z+2)}\phi_d(k,i). \tag{36}$$

The convolution of Eq. (36) with $C(k,j)$ gives

$$\begin{aligned}&C(j,k)*S(k,l)*C(l,i) \\ &\quad=\frac{z(1-4z)}{[(1+2z)(1-z)]^2(z+2)} \\ &\quad\times\rho(1+B/3)\int_{z_k<0}\phi_d(k,j)\phi_d(k,i)dk.\end{aligned} \tag{37}$$

In addition to $S(k,l)$ in which $k=l$, we must also consider the case where only one field point is inside the wall ($k=l$) as shown in Fig. 5(b). It gives

$$\frac{1}{[(1+2z)(1-z)]^2}\rho(1+B/3)\int_{z_k<0}\phi_d(k,j)\phi_d(k,i)dk. \tag{38}$$

Then, by adding Eqs. (37) and (38) we get

$$\begin{aligned}&\frac{2(1+z-2z^2)}{[(1+2z)(1-z)]^2(z+2)} \\ &\quad\times\rho(1+B/3)\int_{z_k<0}\phi_d(k,j)\phi_d(k,i)dk.\end{aligned} \tag{39}$$

When $i=j=1$, the integral in Eq. (39) is identical to the one calculated at low density and the result is simply

$$\frac{-3\beta\mu^2z(1+z-2z^2)}{16[(1+2z)(1-z)]^2(z+2)}(1+B/3)^2(1+\cos^2\theta_1)\frac{1}{z_1^3}. \tag{40}$$

In Eq. (40), we have taken into account the symmetry number

(1/2) of the ring and introduced the factor $(1+B/3)^2$ discussed in Sec. III B. By using Eqs. (21) and (22), expression (40) can be put in a more transparent form, we have

$$-\frac{\beta\mu^2}{16}\frac{(\epsilon-1)}{\epsilon(\epsilon+1)}\left(\frac{\epsilon-1}{3y}\right)^2(1+\cos^2\theta_1)\frac{1}{z_1^3}, \tag{41}$$

In the case where i,j, and 1 are related via the triplet direct correlation function, we are led to calculate the integral

$$\int_{z_k<0}\phi_d(k,j)c(1,i,j)\,\phi_d(k,i)dk\,di\,dj. \tag{42}$$

This calculation can be considerably simplified by using some arguments based both on the symmetry and on the range of the various functions contained in Eq. (42). By construction $c(1,i,j)$ is such that i and j are at least doubly connected. Moreover, due to the parity selection rule, at least three f^l bonds must start from i or j. Thus, $c(1,i,j)$ is certainly short ranged and it is a bulk quantity. Accordingly, in Eq. (42), we may replace $\mathbf{r}_{ki}$ by $\mathbf{r}_{k1}$ and $\mathbf{r}_{kj}$ by $\mathbf{r}_{k1}$. The field points i and j are now disconnected from the long-range bond. We may go further in the calculation of Eq. (42) by performing explicitly the integration over orientations of i and j and l. In order to do that, it is convenient to expand $c(1,i,j)$ as

$$c(1,i,j)=\sum_{L_1L_2L}^{M_1M_2M}Y_{L_1}^{M_1}(\hat{\mu}_i)Y_{L_2}^{M_2}(\hat{\mu}_j)Y_L^M(\hat{\mu}_1)C_{L_1L_2L}^{M_1M_2M}(r_{1i},r_{1j}), \tag{43}$$

where the function Y_l^m represents the usual spherical harmonic defined with standard phase convention.[22] When the explicit expression of $\phi_d(l,i)$ is introduced in Eq. (42), the addition theorem[22] and an extensive use of the orthogonality of the spherical harmonics lead to

$$\left(\frac{4\pi}{3}\beta\mu^2\right)^2\int d\mathbf{r}_i\,d\mathbf{r}_j\,d\mathbf{r}_{k1}\,\frac{1}{r_{ki}^6}\sum_{L,M}Y_L^M(\hat{\mu}_1)$$
$$\times\sum_m C_{11L}^{mmM}(\mathbf{r}_{1i},\mathbf{r}_{1j})\left[1+4\pi Y_1^m(\mathbf{r}_{k1})Y_1^m(\mathbf{r}_{k1})\right]. \tag{44}$$

The integration over $\mathbf{r}_{k1}$ requires only the use of elementary functions and Eq. (44) can be written as

$$\frac{\pi}{2z_1^3}\left(\frac{4\pi}{3}\beta\mu^2\right)^2\sum_{L,M}Y_L^M(\mu_1)$$
$$\times\sum_m\left(1-\frac{\delta_{m\pm1}}{2}\right)\int C_{11L}^{mmM}(r_{1i},r_{1j})d\mathbf{r}_i\,d\mathbf{r}_j, \tag{45}$$

where $\delta_{m\pm1}$ is the usual Kronecker delta. Finally, the contribution of the triplet direct correlation function to the ring is given by

$$-\frac{\beta\mu^2}{8z_1^3}\frac{(1+z-2z^2)z}{(1+2z)^2(z+2)}$$
$$\times\left(\frac{1+B/3}{1-z}\right)^2\sum_{L,M}Y_L^M(\hat{\mu}_1)\alpha(L,M), \tag{46}$$

where we have defined

$$\alpha(L,M)=\frac{\rho^2}{4\pi}\sum_m\left(1-\frac{\delta_{m+1}}{2}\right)\int C_{11L}^{mmM}(\mathbf{r}_{1i},\mathbf{r}_{1j})d\mathbf{r}_i d\mathbf{r}_j. \tag{47}$$

Now, regrouping Eqs. (40) and (46) we get

$$\rho_{\text{ring}}(1)=-\frac{\beta\mu^2}{16}\frac{(\epsilon-1)}{\epsilon(\epsilon+1)}\left(\frac{\epsilon-1}{3y}\right)^2\frac{1}{z_1^3}$$
$$\times\left[1+\cos^2\theta_1+\sum_{L,M}Y_L^M(\hat{\mu}_1)\alpha(L,M)\right]. \tag{48}$$

Since $\rho_{\text{ring}}(1)$ is a part of $\rho(1)$, the properties of symmetry [see, for instance, Ref. 7) imply that L is even and $M=0$. Expression (48) can be also written as

$$\rho_{\text{ring}}(1)=-\frac{\beta\mu^2}{16}\frac{(\epsilon-1)}{\epsilon(\epsilon+1)}\left(\frac{\epsilon-1}{3y}\right)^2\frac{1}{z_1^3}\sum_l Y_{2l}^0(\hat{\mu}_1)\gamma(2l) \tag{49}$$

with

$$\gamma(0)=\frac{4\pi}{3}\sqrt{4\pi}+\alpha(0,0),$$
$$\gamma(2)=\frac{2}{3}\sqrt{\frac{4\pi}{5}}+\alpha(2,0), \tag{50}$$
$$\gamma(2n)=\alpha(2n,0)\quad(n>1).$$

The final step in our calculation consists in calculating the convolution of $\rho_{\text{ring}}(1)$ with the total pair correlation function as discussed in Sec. III C. Here, we have essentially to consider the integral

$$\int\frac{1}{z_2^3}\sum_l Y_{2l}^0(\mu_2)\gamma(2l)h(2,1)d2. \tag{51}$$

We see that Y_{2l}^0 selects in the angular expansion of $h(1,2)$ the terms of parity $2l$. These terms are orthogonal to the long-range part of $h(1,2)$ which is proportional Y_1^m. Thus, in Eq. (51), the relevant part of $h(1,2)$ is short ranged. $h(1,2)$ is a bulk quantity that we may expand in invariant rotationals in the usual way[22]

$$h(1,2)=\sum_{l_1l_2L}^{m_1m_2m}h_{l_1l_2L}(r_{12})C(l_1l_2L;m_1m_2m)$$
$$\times Y_{l_1}^{m_1}(\hat{\mu}_1)Y_{l_2}^{m_2}(\hat{\mu}_2)Y_L^{m*}(\hat{r}_{12}), \tag{52}$$

where $C(l_1l_2L;m_1m_2m)$ is a Clebsh–Gordan (CG) coefficient. The calculation of Eq. (51) can be performed exactly as was the one corresponding to $\rho_{2,2}(1)$ studied in Sec. II, and we may use the arguments developed in Appendix B [see Eq. (B8)]. We replace z_2 by z_1 and Eq. (51) becomes

$$\frac{1}{z_1^3}\int\sum_l Y_{2l}^0(\hat{\mu}_2)\gamma(2l)\sum_{l_1l_2L}^{m_1m_2m}h_{l_1l_2L}(r_{12})C(l_1l_2L;m_1m_2m)$$
$$\times Y_{l_1}^{m_1}(\hat{\mu}_1)Y_{l_2}^{m_2}(\hat{\mu}_2)Y_L^m(\hat{r}_{12})d2. \tag{53}$$

The integration over the spatial coordinates implies $L=0$ and $m=0$ while the integration over the molecular orientation selects $l_2=2l$ and $m_2=0$. The selection rules on the CG coefficient lead to $l_1=l_2=21$ and $m_1=m_2=0$. Thus, the first term in the right-hand side of Eq. (53) becomes

$$\frac{1}{z_1^3}\sum_l\frac{\gamma(2l)}{\sqrt{4\pi(2l+1)}}Y_{2l}^0(\hat{\mu}_1)\int h_{2l,2l,0}(r)d\mathbf{r}, \tag{54}$$

where we have used the explicit expression of the CG coefficients.[22]

The final expression for $\rho(1)$ is deduced from Eqs. (54) and (48). We have

$$\rho(1) = -\frac{\beta\mu^2}{16}\frac{(\epsilon-1)}{\epsilon(\epsilon+1)}\left(\frac{\epsilon-1}{3y}\right)^2\frac{1}{z_1^3}\sum_l Y^0_{2l}(\hat{\mu}_1)\gamma(2l) \times\left[1+\frac{\rho}{\sqrt{4\pi(2l+1)}}\int h_{2l,2l,0}(r)d\mathbf{r}\right]. \quad (55)$$

This equation represents our main result. We call $\rho(1)$ the "exact profile" because, by pictorial arguments, we have verified that the addition of an extra bond to the graphs considered previously can not contribute to the long tail of $\rho(1)$, or if it does, then the new graph is not topologically different from the previous ones.

The general result (55) will be discussed in Secs. V and VI. First, we will consider the component corresponding to $l=0$, which is independent of the molecular orientation and gives us the long-range tail of the density profile $\rho^0(z_1)$. The angular distribution will be analyzed in the last section.

V. THE DENSITY PROFILE $\rho^0(z_1)$. RELATION WITH THE ELECTROSTRICTION PHENOMENA

The density profile can be written as

$$\rho^0(z_1) = -\frac{\beta\mu^2}{16}\frac{(\epsilon-1)}{\epsilon(\epsilon+1)}\left(\frac{\epsilon-1}{3y}\right)^2 4\pi\gamma(0) \times\left[1+\frac{\rho}{4\pi}\int h_{000}(r)d\mathbf{r}\right]\frac{1}{z_1^3}. \quad (56)$$

With the definition (52), the quantity in square brackets is nothing less than $\rho\chi/\beta$, where χ is the isothermal compressibility.[8] The coefficient $\gamma(0)$, given in Eq. (50), is determined by $\alpha(0)$ which we may calculate from Eq. (47). We have

$$\alpha(0,0) = \frac{\rho^2}{4\pi}\sum_m\left(1-\frac{\delta_{m\pm1}}{2}\right)\int C^{mm0}_{110}(\mathbf{r}_{1i},\mathbf{r}_{1j})d\mathbf{r}_i\, d\mathbf{r}_j. \quad (57)$$

The component C^{mm0}_{110} of the triplet direct correlation function is obtained by the functional derivative of the direct pair correlation function c^{mm}_{11}. We have

$$C^{mm0}_{110}(\mathbf{r}_{1i},\mathbf{r}_{1j}) = \int\frac{\delta C^{mm}_{11}(\mathbf{r}_{1i})}{\delta\rho(j)}d\Omega_j. \quad (58)$$

Instead of C^{mm}_{11} it is more usual to introduce the function noted c^{110}, classically used in the theory of polar fluids.[22] From the definition (43), we can see that $C^{mm}_{11}(r) = 4\pi/3c^{110}(r)$. By using the properties of the functional derivative we get[20]

$$\int C^{mm0}_{110}(\mathbf{r}_{1i},\mathbf{r}_{1j})d\mathbf{r}_{1i} = \frac{4\pi}{3}\frac{\partial c^{110}}{\partial\rho}(r_{1j}) \quad (59)$$

and finally

$$\int C^{mm0}_{110}(\mathbf{r}_{1i},\mathbf{r}_{1j})d\mathbf{r}_{1i}\, d\mathbf{r}_{1j} = \frac{4\pi}{3}\frac{\partial}{\partial\rho}\int c^{110}(r)d\mathbf{r}. \quad (60)$$

The right-hand side of Eq. (60) can be explicitly calculated by using the exact relation

$$\frac{(\epsilon-1)}{(\epsilon+2)} = \frac{y}{1+(\rho/3)\int c^{110}(r)d\mathbf{r}} \quad (61)$$

first established by Ramshaw.[23] When both sides of Eq. (61) are derived relative to ρ we obtain

$$\frac{\rho^2}{3}\frac{\partial}{\partial\rho}\int c^{110}(r)d\mathbf{r} = -1+\frac{3y\rho}{(\epsilon-1)^2}\frac{\partial\epsilon}{\partial\rho}. \quad (62)$$

From this relation, Eqs. (56) and (57) get

$$\rho^0(z_1) = -\frac{\beta\mu^2}{12}\frac{(\epsilon-1)}{\epsilon(\epsilon+1)}\left(\frac{\epsilon-1}{3y}\right)^2\left[\frac{\rho\chi}{\beta}\right] \times\left(1+\frac{\rho}{3}\frac{\partial}{\partial\rho}\int c^{110}(r)d\mathbf{r}\right) \quad (63)$$

that we may also write in a more compact form

$$\rho^0(z_1) = -\frac{1}{16\pi}\frac{(\epsilon-1)}{\epsilon(\epsilon+1)}\left[\frac{\partial\epsilon}{\partial\rho}\frac{\rho\chi}{\beta}\right]\frac{1}{z_1^3}. \quad (64)$$

In these expressions, we observe the signature of the image potential via the factor $[(\epsilon-1)/\epsilon(\epsilon+1)]/z_1^3$ which is reminiscent of Eq. (1). As expected from the low density analysis, we see also that $\rho^0(z_1)$ is not entirely determined by the image potential.

In order to elucidate the physical meaning of Eqs. (63) and (64), we first isolate in Eq. (63) the contribution

$$\bar{\rho}(z_1) = -\frac{\beta\mu^2}{12}\frac{(\epsilon-1)}{\epsilon(\epsilon+1)}\left(\frac{\epsilon-1}{3y}\right)^2\left[\frac{\rho\chi}{\beta}\right]\frac{1}{z_1^3}. \quad (65)$$

It corresponds to neglecting the effect of the triplet direct correlation function introduced in Sec. III B. This approximation of $\rho^0(z_1)$ can be understood by using the following intuitive arguments. The product $\mu(\epsilon-1)/3y$ represents the classical effective dipole moment μ_{eff} in bulk phase. For instance, we know that the long-range part of $h(1,2)$ can be interpreted as $-\beta$ times the interaction between two effective point dipole–dipole immersed in a dielectric continuum.[15–17] Thus, it seems natural to change μ to μ_{eff} in Eq. (1). In this way we take into account a local rearrangement around each dipole but, clearly we suppose that this environment is identical to the one existing in bulk phase. Thus, it seems reasonable to assume that

$$W(1) = \frac{\mu^2}{16}\frac{(\epsilon-1)}{\epsilon(\epsilon+1)}\left(\frac{\epsilon-1}{3y}\right)^2\left(\frac{1+\cos^2\theta_1}{z_1^3}\right) \quad (66)$$

is a realistic first approximation of the potential of mean force for a dipole in the interfacial region. Accordingly, the mean force exerted on the molecule whatever its orientation is given by

$$F(1) = -\frac{\partial}{\partial z_1}\int W(1)d\Omega_1 = -\frac{\partial}{\partial z_1}\left[\frac{\mu^2}{12}\frac{(\epsilon-1)}{\epsilon(\epsilon+1)}\left(\frac{\epsilon-1}{3y}\right)^2\frac{1}{z_1^3}\right] \quad (67)$$

and the total force by unit volume at the point z_1 is $\rho^0(z_1)F(z_1)$. It is tempting to consider this quantity as an external force created by the surface. Then, in order to preserve the mechanical equilibrium in the interface this force must be balanced by the gradient of pressure $p(z_1)$. Since the phenomenon that we study exhibits a slow spatial variation, a local approximation for $p(z)$ can be sufficient. In this kind of classical approximation, we assume that $p(z)$ is related to $\rho(z)$ in the same way as the bulk pressure p is related to ρ, thus $p(z) = p[\rho(z)]$. When focusing on a region far from the wall the force balance equation can be written as

$$-\rho\frac{\partial}{\partial z_1}\left[\frac{\mu^2}{12}\frac{(\epsilon-1)}{\epsilon(\epsilon+1)}\left(\frac{\epsilon-1}{3y}\right)^2\frac{1}{z_1^3}\right] = \frac{\partial p}{\partial\rho}\frac{\partial\rho^0(z_1)}{\partial z_1}. \quad (68)$$

This equation can be integrated from the bulk to a given point in the interface. Then, using the thermodynamic identity $\partial p/\partial\rho = 1/(\rho\chi)$, we recover immediately expression

(65). Thus, Eq. (65) appears as a consequence of a local force balance in the interface.

Equation (65) can be also written in the form

$$\rho(z_1) = -\frac{\beta\mu^2}{12}\frac{(\epsilon+1)}{\epsilon(\epsilon-1)}\left(\frac{\epsilon-1}{3y}\right)^2\frac{1}{z_1^3} + \int W(2)h_{000}(r_{12})d2. \tag{69}$$

Here, the first term is just the isotropic part potential of mean force defined in Eq. (66). The second term can be interpreted in the spirit of the Ornstein–Zernike equation. It represents the effect on the density at the point 1 due to a molecule 2 which is submitted to the influence of the image potential. In addition to $\rho(z_1)$, we observe that Eq. (63) contains a extra term related to the triplet direct correlation function. This contribution to the profile is a consequence of Eq. (42). This equation represents the situation in which molecule 1 is simultaneously correlated with two molecules in its short-range environment in such a way that we can not reduce these correlations to a product of pair correlations. Clearly, such an effect is beyond the approximation (66) and it can not be present in a model based on a dielectric continuum.

We may also analyze $\rho^0(z_1)$ via Eq. (64). In Eq. (64), the combination of physical parameters in square brackets, generally noted K_h, appears when we study the equilibrium density of an homogeneous polar fluid in an electric field (see for instance Refs. 21, 24, and 25). Then, K_h determines the magnitude of the so called electrostriction effect. However, we must point out that the problem investigated here differs from the classical electrostriction on two points. First, as opposed to what happens in homogeneous liquids, K_h governs a lowering in the density. This is expected from Eq. (67) which shows us that the image force $F(z_1)$ is repulsive and tends to push the molecules towards the bulk phase. Secondly, we have no external electric field. Nevertheless, besides these qualitative differences, the presence of K_h suggests that a strong analogy must exist between our calculation and the theory of electrostriction. Previously, in Sec. III B, we have interpreted Fig. 4 as representing various kinds of coupling between 1 and the "wall." The bonds emerging from the wall and arriving at i and j in the liquid side act as a probe which allows us to explore the neighborhood of 1. In the case of classical electrostriction the situation is similar, except that the wall is now charged and we may directly investigate the bulk phase by an electric field. This explains why the asymptotic behavior of the profile and the electrostriction are determined by the same constant K_h. We may interpret Eq. (64) as the result of a "natural electrostriction phenomena" induced by the image force.

As in the case of the electrostriction, the exact result (64) includes some bridge diagrams and accordingly it cannot be obtained by considering the wall–particle hypernetted chain equation.

In the last section we will analyze the orientational structure far from the wall.

VI. ORIENTATIONAL STRUCTURE

In Eq. (55), we first examine the term corresponding to $l=1$. It can be written as

$$\rho_{l=1}(1) = -\frac{\beta\mu^2}{16}\frac{(\epsilon-1)}{\epsilon(\epsilon+1)}\left(\frac{\epsilon-1}{3y}\right)^2 P_2(\cos\theta_1)\sqrt{\frac{5}{4\pi}}\,\gamma(2) \times\left[1+\frac{\rho}{\sqrt{5.4\pi}}\int h_{220}(r)d\mathbf{r}\right]\frac{1}{z_1^3}, \tag{70}$$

where we have used the relation between Y^0_{2l} and the second Legendre polynomial $P_2(\cos\theta_1)\cdot\gamma(2)$ is given in Eq. (50). We may discuss Eq. (70) as in the case of the density profile.

If we neglect the pair correlation contribution ($h_{220}=0$) and the triplet direct correlation function [$\alpha(2,0)=0$ in Eq. (50)], then the coefficient of $P_2(\cos\theta_1)$ in Eq. (70) is

$$\int P_2(\cos\theta_1)W(1)d\Omega_1. \tag{71}$$

This quantity represents the alignment[22] of 1 relative to the normal to the wall, calculated with the potential of mean force defined in Eq. (66). Besides this first effect, we note that the orientational structure of 1 can be also determined by its environment when this one is perturbed by the wall. This leads us to calculate the integral

$$\int P_2(\cos\theta_1)W(2)h(2,1)d2 \simeq -\frac{\beta\mu^2}{16}\frac{(\epsilon-1)}{\epsilon(\epsilon+1)}\left(\frac{\epsilon-1}{3y}\right)^2\frac{1}{z_1^3} \times\int P_2(\cos\theta_1)P_2(\cos\theta_2)h(2,1)d2. \tag{72}$$

After performing the integration over the orientations, we can see that Eq. (72) is determined by the function h_{220}. When Eqs. (71) and (72) are added we recover the term in square brackets in Eq. (70). It represents the dipolar contribution to the Kerr constant.[26,27] As in the discussion relative to the density profile, the appearance of this macroscopic quantity is not fortuitous. The asymptotic behavior of the profile and the Kerr effect are determined by the same function characterizing the alignment of dipoles. This alignment is observed via an external electric field in the case of the usual Kerr effect and it is naturally induced by the image potential in the interfacial region.

As discussed above, the triplet direct correlation function introduces a more sophisticated coupling in which three particles of the liquid are simultaneously implied. We may note that this function also introduces in Eq. (70) some terms having a symmetry of higher order ($l>2$). Clearly, these last contributions to the orientational structure are far beyond the dielectric continuum model.

ACKNOWLEDGMENTS

The author is grateful to Dr. M. L. Rosinberg, Dr. V. Russier, and Dr. W. Dong for very interesting discussions.

APPENDIX A: DEFINITION OF ϕ_d AND TRANSFORMATION OF f^l

The function f^l defined in Eq. (9) can be transformed in a more tractable expression as proposed in Ref. 7. In the calculations, $f^l(i,j)$ appears via some integrals such as

$$I=\int f^l(i,j)G(j,k)dj, \tag{A1}$$

where the function $G(i,j)$ results, for instance, from a previous graph calculation and dj denotes an integration on spatial and orientational coordinates of j (for convenience a factor $1/4\pi$ is included in dj). When Eq. (9) is used, Eq. (A1) can be written as[7]

$$I = -\beta\mu^2(\hat{\mu}_i\cdot\nabla_i)\int\theta(r_{ij}-\lambda)(\hat{\mu}_j\nabla_j)(1/r_{ij})G(j,k)dj$$

$$+\beta\mu^2\int(\hat{\mu}_i\cdot\hat{r}_{ij})(\hat{\mu}_j\cdot\hat{r}_{ij})[\delta(r_{ij}-\lambda)/r_{ij}^2]G(j,k)dj. \quad \text{(A2)}$$

In the first integral, the integrand is well defined everywhere and we may drop $\theta(r_{ij}-\lambda)$. We consider now

$$-\beta\mu^2(\hat{\mu}_i\cdot\nabla_i)\int(\hat{\mu}_j\cdot\nabla_j)(1/r_{ij})G(j,k)dj \quad \text{(A3)}$$

as the result of the distribution ϕ_d. [See Eq. (10) when operating on $G(j,k)$.]

In homogeneous systems, after performing the integration over the orientations of $\mathbf{r}_{ij}$, the second integral in Eq. (A2) can be transformed into

$$(4\pi\beta\mu^2/3)\int\hat{\mu}_i\hat{\mu}_j[\delta(r_{ij})/r_{ij}^2]G(j,k)dj. \quad \text{(A4)}$$

Thus, $f^l(i,j)$ can be defined in terms of distributions as

$$f^l(i,j) = \phi_d(i,j) + (4\pi\beta\mu^2/3)\,\hat{\mu}_i\cdot\hat{\mu}_j[\delta(r_{ij})/r_{ij}^2]. \quad \text{(A5)}$$

This expression becomes slightly more complicated in inhomogeneous systems where the last term in Eq. (A5) takes a tensorial character in the neighborhood of the wall.[7] Such a sophistication is unnecessary in the present paper.

APPENDIX B: MATHEMATICAL ORIGIN OF THE LONG TAIL OF ρ(1)

In this Appendix, we show to what conditions a function $G(r)$ can contribute to the long tail of the profile. In this respect, the dependence on the molecular orientations is not essential and we are basically concerned by some integrals as

$$I = \int\rho(z_2)G(r_{12})d\mathbf{r}_2. \quad \text{(B1)}$$

For example, in the calculation of $\rho_1(1)$, we have $\rho(z_2) = \theta(z_2) - 1$ and $G(r_{12}) = 1/r_{12}^6$.

In the calculation of Eq. (B1), we first consider the part I_w corresponding to the integration domain defined by $z_2 < 0$. By changing the variables, I_w becomes

$$I_w = -2\pi\int_{-\infty}^{-z_1}dz_{12}\int_{|z_{12}|}^{\infty}dr_{12}\,r_{12}G(r_{12}) \quad \text{(B2)}$$

that we may also rearrange as

$$I_w = -2\pi\int_{z_1}^{\infty}\int_{2}^{\infty}dr\,rG(r). \quad \text{(B3)}$$

After an integration by parts, we get

$$I_w = -2\pi\int_{z_1}^{\infty}dr\,r^2G(r) + 2\pi z_1\int_{z_1}^{\infty}dr\,rG(r)$$

$$-\lim_{z\to\infty}2\pi z\int_{z}^{\infty}dr\,rG(r). \quad \text{(B4)}$$

For functions $G(r)$ decreasing more rapidly than $1/r^3$ for large values of r, the last term vanishes. From Eq. (B4), we can see that I_w is $\sim 1/z_1^3$ provided that $G(r)$ behaves as $1/r^6$ when $r > z_1$.

Now, we analyze the case where 2 is on the liquid side but remains in a region of finite thickness L located near the wall. We will assume that in this region $\rho(z_2)$ is nearly constant or bounded by M. Thus, we consider

$$I_L = 2\pi\int_{-z_1}^{-z_1+L}dz_{12}\,M\int_{|z_{12}|}^{\infty}dr_{12}\,r_{12}G(r_{12}). \quad \text{(B5)}$$

That we may write in a form similar to Eq. (A4),

$$I_L = 2\pi M\left[\int_{z_1-L}^{z_1}dr\,r^2G(r) + z_1\int_{z_1}^{\infty}dr\,rG(r)\right.$$

$$\left.-(z_1-L)\int_{z_1-L}^{\infty}dr\,rG(r)\right]. \quad \text{(B6)}$$

In the limit $z_1\to\infty$, while $L/z_1\to 0$, we expand the integral in a power series of L/z_1. We get

$$I_L = 2\pi M\left[-2(L/z_1)\,z_1^3G(z_1)\right.$$

$$\left.+(L/z_1)z_1\int_{z_1}^{\infty}dr\,rG(r)\right]. \quad \text{(B7)}$$

Thus, if $G(r)\simeq 1/r^6$ for large r, then I_L is $\sim 1/z^4$ and this integral does not contribute to the long tail of $\rho(1)$. This situation is encountered, for instance, in the calculation of $\rho_{2,1}(1)$ in Sec. II.

Finally, we will focus on the case in which $\rho(z_2)$ is $\sim A/z_2^3$ when $z_2 > L$. This problem occurs in the calculation of $\rho_{2,2}(1)$, $\rho_{2,2}(2)$, and more generally in the convolution introduced in Sec. III C and investigated in Sec. IV B. Now, we have to calculate

$$I_\infty = 2\pi\int_{-z_1+L}^{\infty}dz_{12}\frac{A}{(z_1+z_{12})^3}\int_{|z_{12}|}^{\infty}dr_{12}\,r_{12}G(r_{12}). \quad \text{(B8)}$$

For calculating the asymptotic behavior of this integral we will work in the spirit of the γ- ordering method.[9] We consider the limit $z_1 > 1/\gamma$ while $\gamma\to 0$ and $L/z_1\to 0$. If $I_\infty = 1/z_1^3$ then I_∞ is also given by $\gamma^3/\tilde{z}_1^3$ where $\tilde{z}_1 = \gamma z_1 > 1$. When γ is introduced in Eq. (B8) we get

$$I_\infty = 2\pi\gamma^3A\int_{-(1/\gamma)(\tilde{z}_1+\gamma L)}^{\infty}dz_{12}$$

$$\times\frac{1}{(\tilde{z}_1+\gamma z_{12})^3}\int_{|z_{12}|}^{\infty}dr_{12}r_{12}G(r_{12}). \quad \text{(B9)}$$

In a domain in which $\gamma z_{12}\ll 1$, Eq. (B9) becomes in the limit $\gamma\to 0$,

$$I_{\infty,1} = \frac{2\pi\gamma^3A}{z_1^3}\int_{-\infty}^{+\infty}dz_{12}\int_{|z_{12}|}^{\infty}dr_{12}\,r_{12}G(r_{12}) \quad \text{(B10)}$$

which is nothing less than

$$I_{\infty,1} = \frac{\gamma^3}{z_1^3}A\int d\mathbf{r}\,G(r), \quad \text{(B11)}$$

where the integration is now performed on the overall space.

When $z_{12} > 1/\gamma$, we change the variables z_{12} in $z = \gamma z_{12}$ and r_{12} in $r = \gamma r_{12}$. We obtain

$$I_{\infty,2} = 2\pi A\int_{-\tilde{z}_1}^{\infty}dz\frac{1}{(\tilde{z}_1+z)^3}\int_{|z|}^{\infty}dr\,rG(r,\gamma). \quad \text{(B12)}$$

If $G(r)$ is $\sim 1/r^n$ for large values of r, then $I_{\infty,2}$ is of $O(\gamma^n)$. Thus, except in the case $G(r)\sim 1/r^3$, $I_{\infty,2}$ does not contribute to the long tail of $\rho(1)$ and I_∞ is just given by Eq. (B11). This justifies, for instance, the calculation of $\rho_{2,2}(1)$ presented in Sec. II.

APPENDIX C: CALCULATION OF $\rho_{2,5}(1)$

Here, we want to calculate the function $\rho_{2,5}(1)$ corresponding to the graph shown in Fig. 2(d). We first perform the integration on the field point 2. This requires us to evaluate

$$I = -\rho \int_{z_2<0;z_3<0} f^l(1,2) f^l(1,3)\, d2. \tag{C1}$$

Since 2 and 1 are never on the same side of the interface, $f^l(1,3)$ is reduced to $\phi_d(1,3)$ and from the definitions of f^l in terms of distributions (9), (10), (A3), and (A5) we may write Eq. (C1) as

$$I = -\rho(\beta\mu^2)^2(\hat{\mu}_i\nabla_1)(\hat{\mu}_3\cdot\nabla_3) \times \int d2 \left(\hat{\mu}_2\cdot\nabla_2\frac{1}{r_{12}}\right)\left(\hat{\mu}_2\cdot\nabla_2\frac{1}{r_{32}}\right) + \rho(\beta\mu^2)\hat{\mu}_i\cdot\nabla_1 \times \int d2\,\frac{4\pi\beta\mu^2}{3}\hat{\mu}_3\cdot\hat{\mu}_2\frac{\delta(r_{23})}{r_{23}^2}\hat{\mu}_2\nabla_2\frac{1}{r_{23}}. \tag{C2}$$

The last integral in Eq. (C2) immediately gives $-y\phi_d(1,3)$. For calculating the first integral we perform the integration on the molecular orientations, this leads to

$$\int\left(\hat{\mu}_2\cdot\nabla_2\frac{1}{r_{12}}\right)\left(\hat{\mu}_2\cdot\nabla_2\frac{1}{r_{32}}\right)d2 = \frac{1}{3}\int\left(\nabla_2\frac{1}{r_{12}}\right)\cdot\left(\nabla_2\frac{1}{r_{32}}\right)d\mathbf{r}_2. \tag{C3}$$

This quantity can be calculated by transverse Fourier transform. We have

$$\frac{1}{3}\int e^{iK R_{13}}\int\left(\nabla_2\frac{1}{r_{12}}\right)\left(\nabla_2\frac{1}{r_{32}}\right)d\mathbf{r}_2\, d\mathbf{R}_{13} = \frac{1}{3}\int\left(iK\frac{2\pi}{k}e^{K|z_{12}|} + z\frac{2\pi}{K}\frac{\partial}{\partial z_2}e^{K|z_{12}|}\right) \times\left(iK\frac{2\pi}{K}e^{K|z_{32}|} + z\frac{2\pi}{K}\frac{\partial}{\partial z_2}e^{K|z_{32}|}\right)dz_2, \tag{C4}$$

where $\mathbf{R}_{13}$ is the projection of $\mathbf{r}_{13}$ in the plane $z=0$. To derive Eq. (C4), we have used the well known result

$$\int e^{i\mathbf{K}\mathbf{R}_{12}}\frac{1}{r_{12}}d\mathbf{R}_{12} = \frac{2\pi}{K}e^{K|z_{12}|}. \tag{C5}$$

The right-hand side of Eq. (C4) can be calculated easily and after a back transformation, we have

$$\frac{1}{3}\int d\mathbf{r}_2\left(\nabla_2\frac{1}{r_{12}}\right)\left(\nabla_2\frac{1}{r_{32}}\right) = \frac{1}{3}\frac{2\pi}{r_{13}}. \tag{C6}$$

Finally, by adding the results of each integral in Eq. (C2), we obtain

$$I = \frac{y}{2}\phi_d(1,3). \tag{C7}$$

When the direct $\phi_d(1,3)$ bond [see Fig. 2(d)] is taken into account, then 3 and 1 are doubly connected just as in Fig. 2(a). Accordingly, the final result is

$$\rho_{2,5}(1) = -\frac{3y^2}{64}\beta\mu^2(1+\cos^2\theta_1)\frac{1}{z_1^3}. \tag{C8}$$

[1] D. Levesque and J. J. Weis, J. Stat. Phys. **40**, 29 (1985).
[2] J. P. Badiali, Mol. Phys. **55**, 939 (1985).
[3] J. P. Badiali and M. E. Boudh'hir, Mol. Phys. **53**, 1399 (1984).
[4] W. Dong, M. L. Rosinberg, A. Perera, and G. Patey, J. Chem. Phys. **89**, 4994 (1988).
[5] H. Reiss, H. L. Frisch, and J. L. Lebowitz, J. Chem. Phys. **31**, 369 (1959).
[6] D. Henderson, F. F. Abraham, and J. A. Barker, Mol. Phys. **31**, 1291 (1976).
[7] J. P. Badiali, J. Chem. Phys. **89**, 2397 (1988).
[8] J. P. Hansen and I. R. McDonald, *Theory of Simple Liquids*, 2nd ed. (Academic, New York, 1986).
[9] G. Stell, *Modern Theoretical Chemistry 5, Statistical Mechanics*, edited by B. Berne (Plenum, New York, 1978).
[10] G. S. Rushbrooke, Mol. Phys. **37**, 761 (1979).
[11] A. D. Buckingham and C. G. Joslin, Mol. Phys. **40**, 1513 (1980).
[12] C. G. Joslin, Mol. Phys. **42**, 1507 (1981).
[13] G. S. Rushbrooke and R. G. Shrubsall, Mol. Phys. **55**, 599 (1985).
[14] D. Jepsen and H. Friedman, J. Chem. Phys. **38**, 846 (1962).
[15] G. Nienhuis and J. M. Deutch, J. Chem. Phys. **55**, 4213 (1971).
[16] G. Nienhuis and J. M. Deutch, J. Chem. Phys. **56**, 1819 (1972).
[17] J. S. Høye and G. Stell, J. Chem. Phys. **64**, 1952 (1976).
[18] H. Friedman, *Ionic Solutions Theory* (Interscience, New York, 1962).
[19] J. L. Lebowitz, G. Stell, and S. Baer, J. Math. Phys. **6**, 1282 (1965).
[20] R. J. Baxter, J. Chem. Phys. **41**, 553 (1964).
[21] J. C. Rasaiah, D. J. Isbister, and G. Stell, J. Chem. Phys. **75**, 4707 (1981).
[22] C. G. Gray and K. E. Gubbins, *Theory of Molecular Fluids* (Clarendon, Oxford, 1984).
[23] J. Ramshaw, J. Chem. Phys. **57**, 2684 (1972).
[24] L. D. Landau and E. M. Lifshitz, *Electrodynamics of Continuous Media* (Pergamon, London, 1960).
[25] J. S. Høye and G. Stell, J. Chem. Phys. **72**, 1597 (1980).
[26] J. D. Ramshaw, D. W. Schaefer, J. S. Waugh, and J. M. Deutch, J. Chem. Phys. **54**, 1239 (1971).
[27] S. Kielich, *Dielectric and Related Molecular Processes*, Specialist Periodical Reports, Vol. 1 (The Chemical Society, Washington, D.C., 1972).